ACS Sustainable Chemistry & Engineering

pubs.acs.org/journal/ascecg

Research Article

Improvement in the Thermomechanical Properties and Adhesion of Wood Fibers to the Polyamide 6 Matrix by Sequential Ball Milling Technique

Adel Jalaee and E. Johan Foster*

Cite This: ACS Sustainable Chem. Eng. 2024, 12, 490−500

Read Online

ACCESS | Metrics & More | Article Recommendations | Supporting Information

ABSTRACT: The engineering thermoplastics industry has largely limited the use of natural fiber reinforcements due to their susceptibility to low-onset thermal degradation and water absorption. Therefore, in order to utilize these economically viable and environmentally friendly materials effectively through common composite fabrication methods such as hot pressing, safeguarding them from thermal degradation becomes essential. This work presents a viable industrially technique called sequential ball milling for processing unbleached softwood kraft pulp fibers (PF) with an engineering thermoplastics polyamide 6 (PA6) with high melting temperatures (>220 °C). An additional eco-friendly modification step that employs ball milling and cellulose nanocrystal (CNC) has been implemented in this study to enhance the mechanical properties of the composites. Special attention is given to fine-tuning key variables, such as milling duration and PF particle size, to produce optimal composites. Leveraging the ability of sequential ball milling to evenly distribute pulp fibers into PA6, a 160% increase in Young's modulus was achieved with the incorporation of 30 wt % PF. Importantly, the introduction of a 5 wt % CNC modifying agent elevated Young's modulus to 4.3 GPa, marking a 187% improvement over unmodified PA6. Diverse techniques, including rheological analyses, thermomechanical evaluations, morphological examinations, and assessments of moisture absorption, were utilized to validate the efficiency of the suggested processing approach and the modification phase.

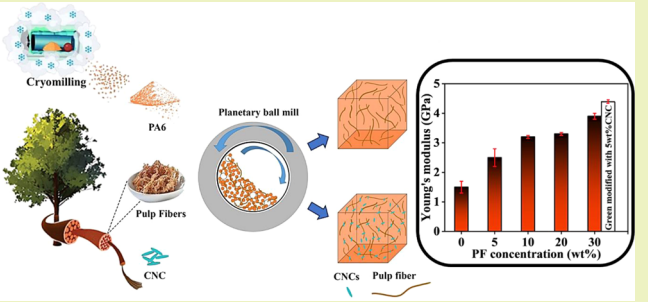

KEYWORDS: *polyamide 6, ball milling, wood fibers, cellulose nanocrystals, biocomposite*

1. INTRODUCTION

Natural fibers, including pulp fibers, have emerged as an appealing resource for the creation of more sustainable short-fiber-reinforced composites, also known as biocomposites.[1,2] The market for biocomposites is already well established, with a reported investment of $22.3 billion in 2019.[3] Pulp fibers are recognized for their potential to serve as mechanical reinforcement and economical filler material, contributing to enhanced dimensional stability for design purposes.[1,4,5] This material has played a pivotal role in the inception of aviation and continues to find utility in light aviation.[1,6] The European automotive sector currently employs 80,000 tonnes of natural fibers as an alternative to synthetic fibers for reinforcing composite components.[7] This trend is anticipated to contribute to the growth of the global biocomposites market during the forecast period. However, a challenge associated with pulp fibers lies in their limited ability to disperse within certain polymers, particularly hydrophobic ones.[5,8,9] Additionally, their lower onset degradation temperature, attributed to their primary cellulose composition, which breaks down beyond 150 °C, poses a constraint.[6,10] This thermal sensitivity poses a challenge to their effectiveness as reinforcements in high melting temperature polymers like polyamide 6 (PA6).[11] PA6, commonly referred to as nylon-6, is a synthetic polymer belonging to the polyamide family. It exhibits a melting temperature of approximately 220 °C and finds extensive use in diverse automotive applications, encompassing engine components, fuel system elements, electrical connectors, structural parts, intake manifolds, engine covers, oil pans, radiator end tanks, and airbag components.[12,13]

One approach to mitigate the issue of thermal degradation is to use chemically modified pulp fibers to improve their dispersion and thermal stability.[14] For example, cellulose fibers can be treated with cross-linking agents or other chemical treatments to improve their thermal stability.[8,15−17] However, there are potential negative effects that must be carefully considered in chemical treatment such as reduced fiber strength, increased production costs and processing steps,

Received: October 2, 2023
Revised: November 28, 2023
Accepted: November 28, 2023
Published: December 13, 2023

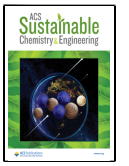

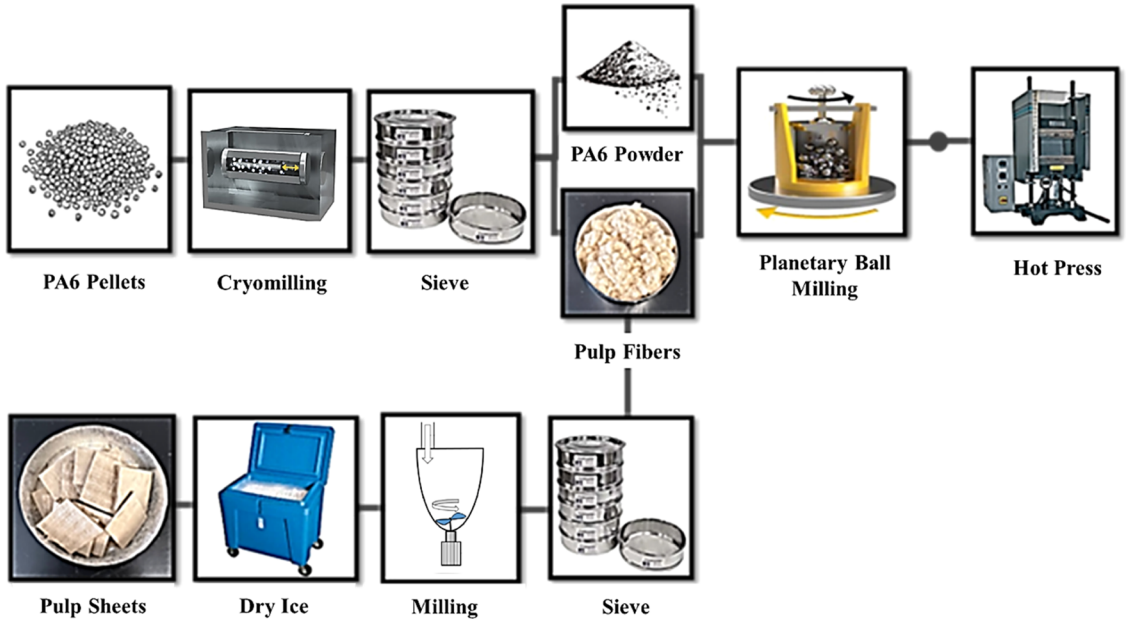

Figure 1. Manufacturing process of the PA6/PFs composite.

environmental impact, and reduced biodegradability.[18] Another approach involves incorporating pulp fibers into the high-melting-temperature matrix using a melt compounding process with lower temperatures and shorter processing times than traditional melt processing, which minimizes the thermal degradation of the pulp fibers.[10,18,19] However, achieving good dispersion of the fibers within the polymer matrix is still problematic with this method.

The promising new technique proposed by our group is based on premixing, cryomilling, and planetary ball milling, which are mechanical processing techniques that are used to embed pulp fibers into polymer particles and improve their thermal stability.[20] Cryomilling is capable of producing finely powdered polymers with a normal distribution in a short period of time. Subsequently, these fine polymer particles are combined with pulp fibers by using planetary ball milling (a process characterized by mild impact energy). Following this, the composite material undergoes the final stages of polymer processing.[6,10,11] In addition to improving the thermal stability of pulp fibers, this process increases the homogeneous dispersion of the fibers within the polymer matrix and increases the surface area of the fibers, which improves the adhesion between the fibers and the polymer matrix.[6]

Careful forethought and meticulous fabrication strategies are necessary to get high-performance composites out of the sequential ball milling method. In other words, the ball milling parameters including milling time, ball size, ball-to-powder ratio, and milling speed heavily impact the performance of the composite.[21] For instance, longer milling times can result in increased breakage, leading to smaller fiber lengths and narrower size distributions, and also lead to the thermal degradation of the fibers and the polymer matrix. Therefore, determining the optimal milling time is crucial in the polymer composite production process.[22,23] So, in the current study to show the viability of our proposed method, we followed the green sequential milling method to include pulp fibers into high-demand PA6 polymer for the anticipated application in the automotive industry.

In a noteworthy advancement, we here introduce a novel green modification approach to enhance the performance of composites. Utilizing sequential ball milling, we have innovatively tailored pulp fibers to achieve enhanced compatibility with the PA6 matrix. Through the strategic use of a cellulose nanocrystal (CNC) modifying agent, we successfully fill the void spaces between the fiber and matrix, thus increasing packing density.[24] This innovative approach not only improves fiber−matrix interaction but also optimizes the dispersion of nanofibers within the PA6 matrix.[25]

In order to elucidate the effectiveness of our proposed sequential ball milling technique and modification process, we conducted a comprehensive study. This investigation considered key variables, including the concentrations of pulp fibers and PA6, as well as milling time. We employed a range of analytical tools, including thermomechanical and rheological analyses, to both characterize the composite materials and underscore the benefits of our environmentally friendly modification approach to the composite's properties.

2. MATERIALS AND METHODS

2.1. Materials. The unbleached softwood kraft pulp (Kappa numbers 23−27) with a crystallinity index (CI) of 70.1% was kindly provided by Canfor Co. (Canada). Industrial grade of PA6, H35ZI (density ρ = 1.13−1.15 g/m^3, pellet form, size of 3 mm), was supplied by AdvanSix and employed as the matrix. Freeze-dried cellulose nanocrystals, CNC (lot no. U38), with a length of 150−200 nm and a diameter of 5−20 nm, a surface charge equal to −50 mV and 90% pure cellulose, 8% hemicellulose, and less than 1% lignin were provided by the University of Maine.

2.2. Pulp Fibers Preparation. The initial cutting of pulp sheets produces pieces of pulp that are then frozen in a dry ice chamber to preserve their properties and to avoid wrapping problems, making them easier to mill. The frozen pulp pieces are then milled using an Ika knife miller (A11, 230VAC, 50/60 Hz) to create uniform pulp fibers. These steps were introduced into the fabrication process to maintain control over the experimental conditions. In real-world industrial applications, they may not be necessary. This type of miller uses a series of sharp blades to cut and grind the pulp pieces into smaller fibers. The pulp fibers were milled using the Ika knife miller for 2 min. To determine the milled pulp fibers size, Sieve analysis was

https://doi.org/10.1021/acssuschemeng.3c06351
ACS Sustainable Chem. Eng. 2024, 12, 490−500

performed using Retsch Analytical Sieve Shaker AS 200 Control for 30 g samples each with a vibration rate of 2 min, amplitude of 2 mm/g, and Vulkollan cubes as a sieving aid.[26]

2.3. Polymer Composites Fabrication Process. *2.3.1. Cryomilling and Planetary Ball Milling.* To prepare the specimens, a two-step ball milling process was employed.[6] In the first step, PA6 pellets were milled using cryomilling (Verder Scientific, Retsch, Germany) with a 55 mL jar and stainless steel beads (20 mm diameter). According to the machine manual, the liquid nitrogen consumption rate was only 0.1 L/min. The grain size specification indicated that after 6 min of milling, 70 ± 5 wt % of particles were smaller than 100 μm. It is important to highlight that, following 6 min of cryomilling PA6 pellets, no substantial alteration in particle size was observed. Therefore, to optimize the energy efficiency, we decided not to continue milling beyond this point. This decision was based on the understanding that prolonged cryomilling did not yield significant size reduction and would, therefore, be an unnecessary energy expenditure.[27]

In the next step, the particles collected via sieve underwent planetary ball milling (PM 400, Retsch, Germany) along with PF or PF and CNC. The planetary ball milling was performed using stainless steel ball-bearing (size of 6.35 mm).

In the initial stage of our study, we selected four different milling times (3, 15, 30, and 60 min) to produce PA6 reinforced with 5 wt % PF and optimized them based on the achieved thermal stability, storage modulus, and Young's modulus. Additionally, we demonstrated the effect of the milling time on the morphology of the PFs. Further details can be found in the Supporting Information.

In the subsequent stage of our study, we produced premixed ball-milled samples of PA6 powder with varying concentrations of PFs (5, 10, 20, and 30 wt %) in optimized milling time (30 min). Furthermore, we introduced three different concentrations of CNC (1, 3, and 5 wt %) to the PA6−30PF composite to obtain samples with optimal mechanical properties. To demonstrate the impact of premixing methods, we used a sample of PA6 reinforced with 30 wt % PF that was prepared without any premixing. This sample was manually mixed by combining the PA6 powder and PF at room temperature in dry conditions for 10 min to prepare samples, and it served as a benchmark for comparison with the premixed samples.

2.3.2. Preparation of Polymer Composite Films. To mold the polymer composite powder into films, we employed a Carver press at 227 °C and a pressure of 2000 psi for 7 min. Spacers were used to regulate the thickness of the films.[6] The fabrication process is illustrated in Figure 1.

Table 1 shows the names and compositions of the samples that were pressed into films. The fabrication process is illustrated in Figure 1.

2.4. Thermomechanical and Rheological Characterization. The thermal stability and onset degradation temperature were evaluated by thermogravimetric analysis using a TGA instrument (TA5500, TA Instruments, DE) operated in the temperature range from 25 to 600 °C with a 20 °C/min heating rate under a nitrogen atmosphere. In addition, differential scanning calorimetry (DSC) (TA Q2000, TA Instruments, DE) was employed to quantify the degree of crystallinity (X_c%) (eq 1). Accordingly, the samples underwent a heat−cool−heat cycle in the temperature range from −30 to 250 °C and a heating/cooling ramp of 10 °C/min. The degree of crystallinity was calculated as follows

$$x_c(\%) = \frac{\Delta H_f}{w \times \Delta H_0} \times 100 \quad (1)$$

where ΔH_f is the experimental heat of fusion from the heating cycle, ΔH_o is the theoretical heat of fusion according to 100% crystalline PA6, which is equivalent to 230 J/g, and w is the weight fraction of PA6 in the sample. Dynamic mechanical thermal analysis (DMTA-850, TA Instruments) was performed in tensile mode, in the temperature range from 0 to 170 °C and a heating rate of 3 °C/min to check the viscoelastic behavior of specimens cut in rectangular shapes. The tensile feature of the samples was investigated by employing an Instron unit 5969 with a 50,000 N load cell (Instron Corporation; Norwood, MA) at a strain rate of 5 mm/min. To this end, melt-pressed films were cut into dog-bone samples according to ASTM D638 (type V).

Rheology experiment was conducted using an MCR702e (Anton Paar) in a frequency sweep range between 600 and 0.1 rad/s at a strain amplitude of 1% followed by a strain sweep test (strain amplitude = 0.1−1000%) at a frequency of 1 rad/s at a temperature of 240 °C. The viscosity of the samples was monitored as a function of shear rate at 240 °C.

2.5. Water Uptake. To determine the water uptake capacity of the composite specimens, we immersed samples measuring 60 × 10 × 1 mm^3 in water at room temperature for 20 days.[22] The weight of the samples was periodically measured after removal of any excess water with tissue paper. The percentage of water uptake at time (t) was calculated using eq 2

$$\text{water uptake } (\%) = \frac{(W_t - W_0)}{W_0} \times 100 \quad (2)$$

where W_0 is the specimen's initial weight and W_t is the weight of the specimens after the immersion time in grams. The mean and standard deviation were calculated for three replicates.

2.6. Morphology. A scanning electron microscope (SEM) (Hitachi S4800, Ibaraki, Japan) operated at an acceleration voltage of 15.0 kV was employed to investigate the cross-sectional morphology of fractured (liquid nitrogen) specimens and assess the interaction between PFs and the PA6 matrix. Accordingly, the cross section of the broken samples was coated with a thin layer of Pt/Pd (2−4 nm) was used a Cressington sputterer. A polarized optical microscope (Nikon Eclipse LV100 polarization microscope (Melville, NY)) was used to visualize the pulp fibers morphology after the ball milling process.

Table 1. Compositions of PA6 Reinforced with PFs and CNCs through 30 min of Premixing Ball Milling, Neat and Hand-Mixed (HM) Control Sample

sample name	PA6 (wt %)	PFs (wt %)	CNC (wt %)
neat PA6	100	0	0
PA6−5PF	95	5	0
PA6−10PF	90	10	0
PA6−20PF	80	20	0
PA6−30PF	70	30	0
PA6−30PF-1CNC	69	30	1
PA6−30PF-3CNC	67	30	3
PA6−30PF-5CNC	65	30	5
PA6−30PF (HM)	70	30	0

3. RESULTS AND DISCUSSION

3.1. Premixing Ball Milling with the Optimized Parameters. Based on the Supporting Information, ball milling time can have an impact on the final dispersion and fiber length, as well as energy consumption and electricity waste.[6,28] Therefore, we optimized the milling time for the PA6 composite reinforced with 5 wt % PF in terms of its thermomechanical properties. Furthermore, we investigated the effects of the milling time on fiber morphology. To achieve this, we selected four milling times (3, 15, 30, and 60 min).[6,11,22] The nomenclature of samples for different milling times is presented in Table S1. Based on the information shown in Figure S1, it can be observed that the sample subjected to 3 min of ball milling exhibits the lowest thermal stability, with an onset thermal degradation temperature of 350 °C. This could be attributed to the low dispersion quality of PF and polymer particles, as they might not have had enough time to form a buffered layer around PFs, which could protect them

https://doi.org/10.1021/acssuschemeng.3c06351
ACS Sustainable Chem. Eng. 2024, 12, 490−500

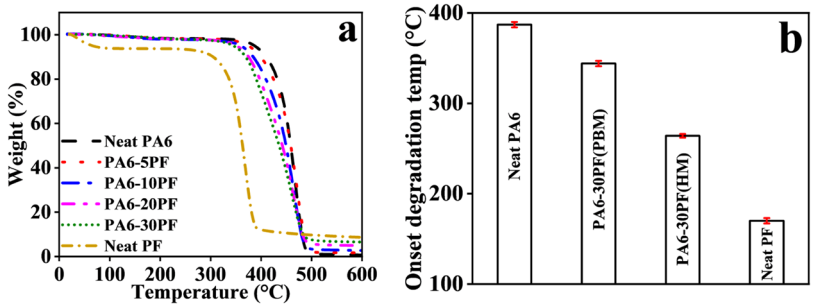

Figure 2. (a) Thermograms of neat PF (pulp fibers), neat PA6, and PA6-PF composites with respect to different PF concentrations. Neat PA6 has higher onset thermal degradation, and PFs incorporation decreases its thermal stability. (b) Comparison of the onset of degradation temperature (5% loss) for the PA6−30PF composite processed via PBM and HM methods. It indicates growth in thermal stability with PBM of 30 wt% PF composite in comparison with the HM process.

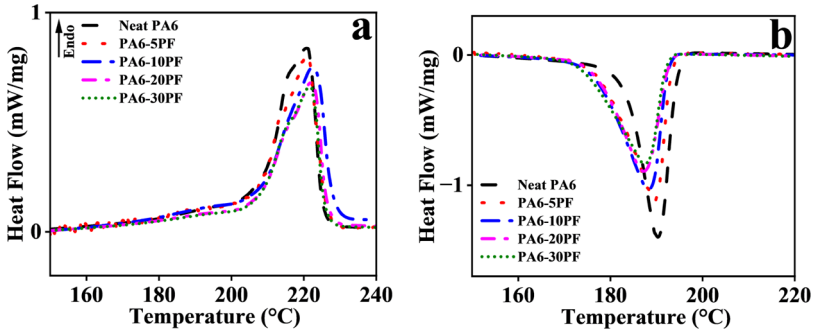

Figure 3. (a, b) DSC thermograms of neat PA6, a polymer composite reinforced with pulp fibers. Heat flow as a function of temperature for samples with a scan rate of 10 °C/min. Thermograms indicate that the composite samples exhibited a lower crystallinity percentage (%X_c) than the neat polymer by increasing the pulp fiber content in the PA6/PFs.

from thermal degradation.[6,11,26] The samples subjected to 15 and 30 min of ball milling show similar thermal stability, while the sample milled for 60 min exhibits a lower thermal stability. This could be due to the excessive ball milling time, which results in smaller fiber fragments with a higher surface area-to-volume ratio. This increased surface area can make the fibers more reactive and susceptible to thermal degradation, leading to a lower onset thermal degradation temperature.[22]

According to Figures S2 and S3, the sample that was premixed for 30 min exhibited the highest storage modulus and Young's modulus at 25 °C. This can be attributed to better dispersion and a lower fiber breaking-through process. Moreover, one-way analysis of variance (ANOVA) was conducted to study the effect of milling time on the thermomechanical properties of the polymer composite at the 0.05 significance level, and the results are shown in Table S2. ANOVA test revealed significant differences between different premixing milling times ($P < 0.05$). Figure S4a,b compare the macroscopic aspect of the composite dog-bone-shaped films that were premixed for 15 and 30 min. The sample premixed for 30 min exhibits significantly better dispersion compared to its counterpart that was premixed for 15 min. The agglomeration of PF in PBM15 is evident and has resulted in a decrease in mechanical properties. The length and aspect ratio of fibers are typically reduced by ball milling, which can lead to negative impacts on the thermomechanical properties if the aspect ratio decreases too much.[22] In Figure S4c,d,e, pictures of PFs in composite samples after 15 and 30 min of ball milling were compared to neat PF before ball milling. ImageJ analysis revealed that the aspect ratio of neat PF was approximately 15, which decreased to 12 and 10 after 15 and 30 min of premixing ball milling, respectively. The fiber width did not change significantly through ball milling, and the length of fibers was approximately 500 and 400 μm after 15 and 30 min, respectively, whereas neat PF had a length of 750 ± 40 μm. Therefore, based on a comparison of the results obtained from thermomechanical analysis and morphology, a milling time of 30 min was selected as the optimized time for making polymer composites in this study.

3.2. Thermal Analysis. Thermogravimetric analysis (TGA) was conducted to study the thermal stability of neat and premixed polymer composites reinforced with PFs at various concentrations (up to 30 wt %). As illustrated by the thermogravimetric curves in Figure 2a, the neat polymeric matrices displayed a degradation profile with a single major weight loss observed at 450 °C, which can be attributed to the degradation of the polymeric backbone.[6,22]

PA6-based composites exhibit two distinct degradation stages: (i) a minor weight reduction attributed to water vaporization, commencing at around 100 °C, linked to the hydrophilic properties of PA6 and the humidity of PFs, and (ii) a main weight reduction phase, occurring between 340 and 460 °C, connected to the thermal degradation of the main chain of PA6 and cellulose, as observed in the PFs' thermograms.[6] Furthermore, the weight loss in this phase corresponds to the different reinforcement loads of the fibers. Other authors have also reported these ternary degradation profiles for PA6-based composites loaded with other cellulose-based fibers.[15,22] When incorporating high quantities of PFs, the onset thermal degradation temperature drops shown in the specific 30 wt % case cause a temperature drop from 387 to 344 °C, due to the conversion of cellulose into acetaldehyde,

https://doi.org/10.1021/acssuschemeng.3c06351
ACS Sustainable Chem. Eng. 2024, 12, 490−500

propenal, methanol, and acetic acid.[29] Espinach et al.[30] explored the thermal properties of polymer composites that were reinforced with bleached kraft softwood. Their findings suggested that the inclusion of a cellulosic filler with lower thermal stability than the polymer matrices was responsible for the reduction in thermal stability observed in the composites.[30]

The presence of a single peak also provides evidence of the relatively strong compatibility between PA6 and the cellulosic fibers. The evidence suggests that ball milling can enhance the interfacial interaction between PFs and the polymer matrix.[22] Figure 2b shows the onset of thermal degradation for a polymer composite sample reinforced with 30 wt % PF, which was prepared by hand mixing and measured after 5 % weight loss. The results were compared to those of the premixed counterpart sample, as well as to neat PA6 and neat PF, which were also measured for onset thermal degradation after 5 wt % weight loss. The premixed sample exhibited an onset degradation temperature of 80 °C higher than that of the hand-mixed sample. According to our previous paper, this observation can be attributed to the thermal buffering effect resulting from the embedding of PFs in PA6 particles.[6] In other words, premixing using ball milling employs collisions between ball bearings to mechanically fuse PFs and polymeric particles in the solid state.[26]

3.3. Crystallization and Thermal Transitions. The mechanical properties of polymer composites are significantly influenced by crystallinity.[31] To assess the impact of pulp fiber fillers on the crystallinity and thermal properties of PA6, DSC measurements were conducted. Figure 3a,b displays the second heating and cooling cycles of the PA6 reinforced with PFs (pulp fibers) composites, while the key characteristic data are summarized in Table 2. Crystalline structures in PA6 can exist as α crystals, γ crystals, or a combination of both. Previous studies have reported that α crystals melt at approximately 220 °C, while γ crystals melt at 214 °C.[32] Interestingly, the addition of PFs resulted in a broadening of the sharp endothermic peak in the PA6 thermogram, suggesting the presence of crystalline structures in both phases.[32] Hence, an increase in the content of PFs implies the development of the γ crystal phase in addition to α crystals.

Table 2. Thermal Analysis Derived and Calculated from Differential Scanning Calorimetry[a]

sample name	T_m (°C)	T_c (°C)	%X_c
neat PA6	221	190	26
PA6−5PF	221	189	27
PA6−10PF	222	188	28
PA6−20PF	223	187	31
PA6−30PF	222	187	33

[a] T_c, crystallization temperature; T_m, melting temperature; X_c, crystallinity.

The DSC results revealed an initial slight decrease in the crystallization temperature (T_c), followed by an increase with a higher pulp fiber content. The melting temperature, taken from the second heating cycle, does not show a significant change. The incorporation of PFs can exhibit dual behavior in the crystallization process of PA6. PFs can act as effective nucleating agents, promoting the formation of additional crystalline regions within the polymer matrix.[25] On the other hand, the addition of PFs may also hinder the molecular mobility of polymer chains, impeding their ability to arrange into well-defined crystalline structures. This restriction in chain mobility can result in a reduction in the overall crystallinity of the polymer matrix.[6,22,33] It is worth noting that the results presented in Table 2 demonstrate an increase in the degree of crystallinity with the addition of PFs. This observation aligns with the findings supporting the notion that pulp fibers effectively act as nucleating agents.[33]

3.4. Morphology of Sample after Ball Milling. Electron microscopy was employed to assess the degree of dispersion and embedment of PFs in the PA6 particles obtained from the premixed ball-milled samples with 30 wt % PF. As depicted in Figure 4a, the PFs were embedded within the polymer particles, and the polymer particles formed a buffer layer around the PFs.[6] This observation is supported by the TGA results presented in Section 3.2, which demonstrate that the onset degradation temperature of the premixed samples was increased. This leads to a higher thermal stability of the polymer composite prior to polymer processing. However, the PFs retained their fibril-like shape, which enhances their reinforcing effect in the polymer matrix even after undergoing ball milling.

The uniform dispersion of PFs among the polymer particles and the absence of visible agglomerates or bundles of micronized fibers in the micrographs of the composite containing 30 wt % PFs confirm the effective dispersion of PFs in the PA6 matrices after premixing. This observation is

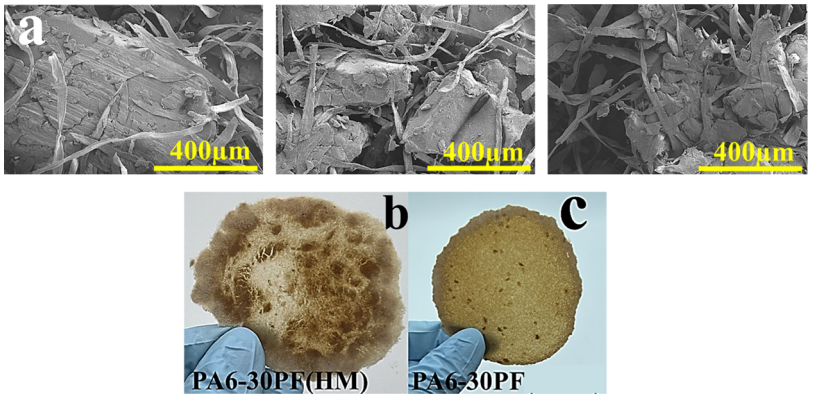

Figure 4. (a) SEM images of PFs embedded within individual PA6 particles. Images are for PA6−30PF composite after 30 min of premixing ball milling. (b, c) Optical photograph images of compression-molded films of PA6−30PF composite prepared by PBM and HM. PBM, premixed ball milling; HM, hand mixing.

https://doi.org/10.1021/acssuschemeng.3c06351
ACS Sustainable Chem. Eng. 2024, 12, 490−500

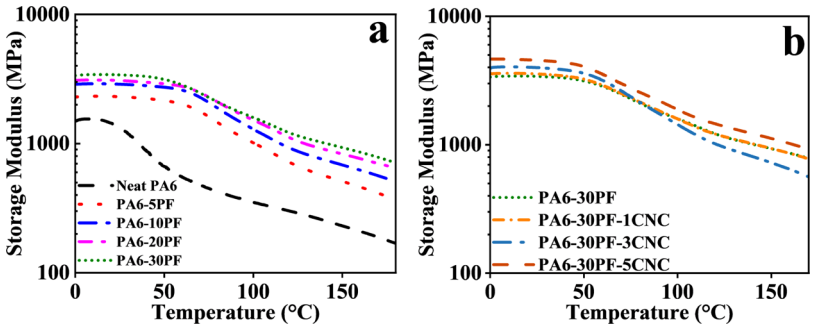

Figure 5. Temperature dependence of storage modulus (E') obtained from DMTA measurements for (a) neat PA6 and PA6/PF composite with respect to different PFs concentrations and (b) PA6−30PF prepared with different concentrations of CNC, after 30 min premixing ball milling.

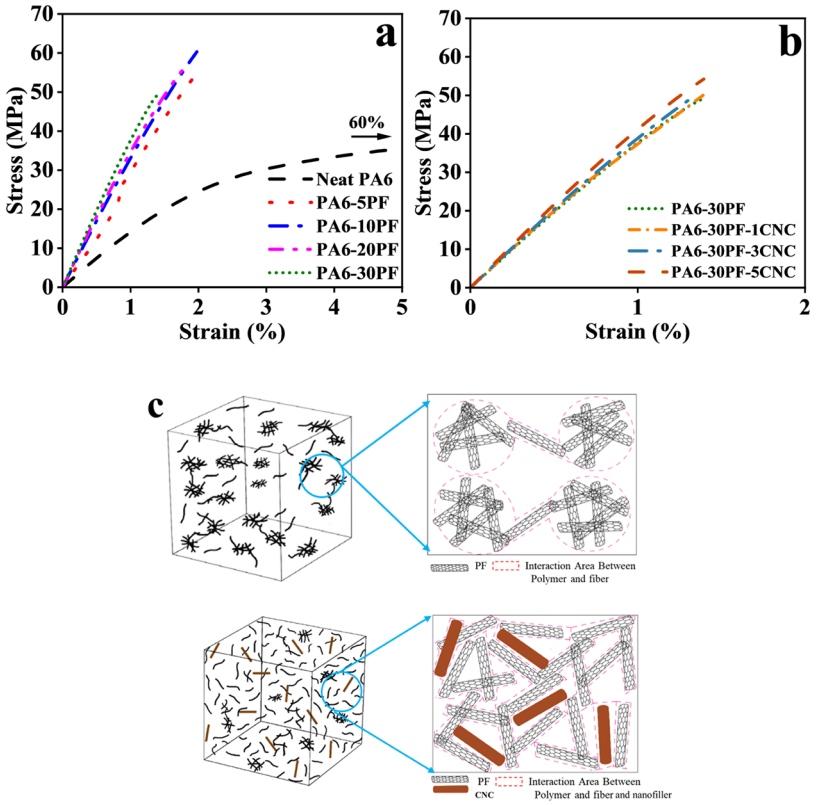

Figure 6. Representative stress−strain curves for (a) neat PA6 and PA6/PF composite with respect to different PFs concentrations, (b) PA6−30PF prepared with different concentrations of CNC, after 30 min premixing ball milling, (c) Schematic of dispersion state of PFs and the interaction area between the polymer and PFs with/without CNC.

consistent with the visual inspection of digital images of compression-molded films presented in Figure 4b,c. Figure 4b clearly shows the agglomeration of PFs in the hand-mixed sample with 30 wt % PF, indicating poor dispersion quality. However, the dispersion was significantly improved after premixing, as depicted in Figure 4c. Moreover, in the hand-mixed samples, the composite film exhibited the presence of voids and fiber pull-outs at the edges. This evidence confirms that premixing is an effective approach to producing high-performance polymer composites.

3.5. Dynamic Mechanical Thermal Analysis. The viscoelastic behavior of the composites was examined using DMA with sinusoidal tensile deformation. DMA measures the storage modulus of composite materials at different temperatures, providing information about their stiffness or resistance to deformation by elastic forces. DMA data also reveal microstructural features, particularly relevant for automotive applications where stiffness is critical. Stiffness depends on both the fibers' reinforcing capability and the matrix's inherent properties.[34]

Figure 5a shows the storage modulus (E') of composite materials at different PF concentrations as a function of temperature. As anticipated, E' values decreased with temperature after the glassy region for all samples. A significant decrease in storage modulus was observed around the glass transition temperature, indicating the rubbery region.[35] By incorporating PFs up to 30 wt % into PA6, the storage modulus (E') values increased, indicating improved stiffness of the composites. The spatial orientation of PFs substantially hinders the mobility of the amorphous phase in PA6, leading to increased stiffness of the composite material.[35] At lower fiber concentrations, the increase in E' values was relatively

https://doi.org/10.1021/acssuschemeng.3c06351
ACS Sustainable Chem. Eng. 2024, 12, 490−500

high because the fibers effectively distributed the stresses across the matrix. This sharing of load between the fibers and the matrix allowed the composite to resist deformation and failure more effectively. However, at higher concentrations of fibers, the increase in storage modulus becomes slower as the fibers begin to interact with each other and form clusters.[36]

It is worth noting that the high shear dispersion techniques employed in this study, such as premixing ball milling, achieved a high level of PF dispersion in the polymer matrix up to 30 wt %. However, we presume that beyond this concentration, the PA6 matrix cannot penetrate and sufficiently wet the PFs under melt compression, resulting in the formation of an inhomogeneous polymer film with weak interfaces between PA6 and PFs. Therefore, it is practically impossible to produce a proper film with PF concentrations exceeding 30 wt %.

To improve the mechanical properties of PA6−30PF and overcome the issue of poor dispersion at higher PF concentrations, three different concentrations of CNCs were introduced as a second filler. As shown in Figure 5b, the addition of 5 wt % CNCs resulted in a significant increase in storage modulus by around 1000 MPa. Table 2 shows the storage modulus for all samples at 25 °C. The high surface area-to-volume ratio of CNCs enables them to interact effectively with the polymer matrix and the reinforcing PFs.[1] CNCs can enhance the interfacial adhesion between the PFs and the polymer matrix, resulting in better load transfer and improved mechanical properties.[24] Additionally, the small size of the CNCs allows for more homogeneous dispersion throughout the composite, preventing the formation of voids and defects that can act as stress concentrations and cause premature failure.[1,24] The CNCs can act as additional reinforcement, contributing to the load-bearing capacity of the composite and improving its mechanical properties, such as the storage modulus.[37]

3.6. Mechanical Performance. Figure 6a presents stress−strain diagrams for a polymer composite reinforced with varying concentrations of PFs. The observed increase in Young's modulus can be attributed to the strong interfacial bonding, facilitating the effective load transfer from the PA6 matrix to the reinforcement.[6] The results demonstrate a gradual rise in Young's modulus as the load of PFs increases, consistent with previous research on fiber load effects.[4,5,22] This can be easily explained by the superior stiffness of cellulose-based fibers compared to polymeric matrices.[13] Notably, composites reinforced with 30 wt % PFs exhibited a remarkable 160% increase in Young's modulus compared to PA6 matrices. Unlike numerous studies in the existing literature,[8,15−17,38] this exceptional tensile characteristic was achieved without resorting to expensive or laborious chemical modifications of PFs. The notable improvements were primarily observed in PA6-based composites, supporting the favorable compatibility of the pulp fibers with PA6 when prepared by using the premixing ball milling method. This finding indicates that micronized fibers produced through ball milling still possess substantial reinforcing capabilities despite their reduced sizes.[22] The effectiveness of this reinforcing effect is closely linked to the fibrillar morphology of the micronized fibers, which is retained even after the ball milling process for 30 min. Qiang et al.[39] and Valente et al.[22] conducted studies on the impact of the aspect ratio of wood-based pulp fibers on the mechanical properties of various polymer composites, and both concluded that the loading content has a more significant influence on the mechanical properties than the fiber aspect ratio.[22] Additionally, the premixing ball milling process not only achieved a high-quality dispersion with the micronization of PFs but also ensured a more extensive coverage of PFs by the PA6 matrix. This extensive coverage provided protection to PFs during the high-temperature fabrication and molding processes.

A loading of 30 wt % PFs is considered a "critical loading" due to the reduced dispersion quality and occurrence of phase separation. Above critical loading, the polymer matrix is unable to fully wet the PFs.[37] In Figure 6b, it is interesting to note that by incorporating CNCs up to 5 wt % into the PA6−30PF composite, the Young's modulus increased from 3.9 to 4.3 GPa, without exceeding the processable ranges. These results can be attributed to the relatively good dispersion of the micronized fibers in the presence of CNCs within the polymeric matrices, improving interfacial adhesion as observed by SEM analysis.[16,24] It is well established that the PFs state of dispersion in a polymer matrix has a controlling effect on the final properties of polymer composite. Hybrid structures shown in Figure 6c formed by combining secondary fillers with PFs is a promising approach for better PFs dispersion. For instance, Liu et al.[40] and Dang et al.[41] have shown that the addition of a secondary filler into polymeric matrix improved the dispersion and distribution of CNTs.

Elongation is a measure of the stiffness and ductility. The elongation percentage of polymer composites typically exhibits a wide range of deviations and does not follow a specific trend.[42,43] However, it is generally observed that an increase in fiber content compared to neat PA6 results in a reduction in this parameter. The increase in stiffness and decrease in elongation at break can be attributed to the restriction on polymer chain movements.[24,43] This restriction is believed to be caused by a reduction in the free volume capacity of PA6.[6] In the case of the PA6 composite with 30 wt % PFs, the elongation at break values was below 3%, which is inferior to those of commercial products (4−6%). It is important to note that in industrial applications, commercial plasticizers are often used to enhance the toughness and elongation of polymer composites.[38] However, the primary focus of our study was on investigating the effect of the premixing ball milling method and the concentration of PFs and CNCs alone without considering other parameters such as the impact of plasticizers. Plasticizers are added to polymers to increase flexibility and reduce brittleness by reducing the intermolecular forces between polymer chains.[6] According to Table 3, Young's modulus follows a trend similar to that of the storage modulus obtained by DMTA.

3.7. Rheology. From an industrial perspective, there is significant emphasis placed on the rheological properties as they serve as critical indicators of dispersion quality for achieving optimal mechanical reinforcement.[11,33] In this section, linear rheological tests were conducted on the samples to gain insight into their microstructural features. Linear melt rheological techniques have been extensively employed as an indirect yet robust indicator of the dispersion quality and spatial arrangement of fillers within a filled system's bulk.[44] Within the linear viscoelastic region, interactions between fillers and polymers influence both local motions (Rouse regime) and long-range arrangement (chain reptation) of the polymer chains. These interactions, in turn, have a significant impact on the rheological response over a wide range of frequencies and time scales.[45] Nevertheless, the dominant influence of network formation by the fillers tends to obscure

https://doi.org/10.1021/acssuschemeng.3c06351
ACS Sustainable Chem. Eng. 2024, 12, 490−500

Table 3. Storage Modulus (E'), Young's Modulus, and Ultimate Tensile Strength of All Samples Regarding Different Concentrations of PFs and CNCs at 25°C Obtained from DMTA and Tensile Testing

sample name	storage modulus (MPa)	Youngs' modulus (MPa)	ultimate tensile strength (MPa)
neat PA6	1300 ± 110	1500 ± 200	49 ± 5
PA6−5PF	2300 ± 50	2500 ± 300	53 ± 4
PA6−10PF	2900 ± 90	3200 ± 50	60 ± 4
PA6−20PF	3150 ± 60	3300 ± 50	56 ± 2
PA6−30PF	3400 ± 100	3900 ± 100	49 ± 1
PA6−30PF-1CNC	3550 ± 80	3900 ± 120	48 ± 1
PA6−30PF-3CNC	4000 ± 50	4100 ± 50	49 ± 1
PA6−30PF-5CNC	4500 ± 100	4300 ± 90	54 ± 2

the long-range motions, which can typically be characterized by the slope of the dynamic moduli at extremely small frequencies in the terminal regime. As a result, the dynamics associated with the Rouse relaxation processes become less significant due to the pronounced impact of the filler network formation.[46] As depicted in Figure 7a, the variations in the storage modulus of the samples at high frequencies are minimal, and their moduli tend to converge. Indeed, as the frequency of deformation decreases, the disparity in storage modulus values between the composites with and without nanofillers becomes significantly more pronounced.

Figure 7b illustrates the viscosity curves across shear rates ranging from 0.01 to 100 s^{-1} for select samples representative of the system to characterize the samples under process-relevant conditions. In general, the viscosity of the materials decreased with increasing shear rates, displaying a shear-thinning behavior. The PA6−30PF-5CNC exhibited viscosity similar to or higher than that of PA6−30PF at lower shear rates. However, with increasing shear rates, the PA6−30PF-5CNC's viscosity started to decrease at around 0.6 s^{-1}. The decrease in viscosity at higher shear rates in PA6−30PF-5CNC can be attributed to its higher hydrophilicity, which may lead to degradation.[11] Water absorbed by PA6 from the CNCs could act as a nucleophile, causing hydrolysis of the PA6 peptide linkages, leading to a significant reduction in average molecular mass and an increase in carboxylic and amine end group concentration. Additionally, the hydrophilicity of the CNCs could result in water uptake, further reducing viscosity.[6,11] Moreover, increased thermal degradation and slip effects due to the higher filler content in this sample might also contribute to viscosity reduction. Overall, the addition of CNCs does not push the material beyond processable ranges, indicating that the material remains suitable for processing despite the observed viscosity changes.

3.8. Morphology of Fracture Surface. The mechanical properties of composites are closely tied to the efficient transfer of energy from the polymeric matrix to the fibers. This transfer, in turn, relies on the dispersion of the fibers and the interfacial adhesion between the fibers and the matrix.[6,22] Figure 8a−c presents SEM micrographs of the cross-sectional fracture surfaces of the samples, investigating the impact of premixing methods and the introduction of CNC. Different colors are employed to differentiate between various fiber morphologies on the fracture surface.

In fiber-reinforced composites, intralaminar and interlaminar fractures can occur within the matrix, at fiber−matrix interfaces, and in the fibers themselves.[47] In Figure 8a, the sample without premixing ball milling (PA6−30PF(HM)) exhibits numerous long pulled-out fibers and voids in the cross section (indicated by the blue color). Additionally, visible agglomerates or bundles of PFs are observed in the composite micrographs due to the cellulose-based fibers' strong tendency to stack together when compounded with thermoplastic matrices. Nevertheless, the presence of hydroxyl end groups in PA6 fosters a high degree of compatibility between this matrix and cellulose fibers compared to common thermoplastic matrices such as PP and PE.[22]

In Figure 8b, the cross section of the PA6−30PF sample, produced using premixing ball milling, shows that a noticeable decrease in the number of pulled-out fibers is observed (shown by red color), and there is also a slight deformation in PFs, resulting in the elongation of the PFs under stress. These observations confirm the good dispersion of micronized fibers after ball milling and their successful embedding in the PA6 matrix.

Figure 8c corresponds to sample PA6−30PF-5CNC, where premixing ball milling was also employed. The micrograph reveals that fractured fibers are more prevalent than pulled-out fibers (shown by yellow color), providing further evidence of their compatibility. Moreover, the micrographs suggest a slightly improved compatibility between the fibers and PA6 in the presence of CNC, likely due to enhanced interfacial interaction of PFs with the matrices. The combination of CNCs and PFs enables nanoparticles to fill the gaps between the fibers, enhancing their packing density, resulting in a more homogeneous distribution and improved interfacial interaction of PFs in the PA6 matrix.[6] Hybrid composites benefit from CNCs, as they enhance the dispersion of PFs by reducing the

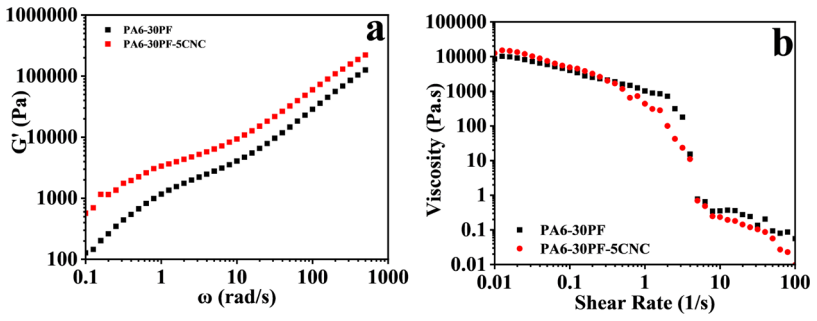

Figure 7. Rheological behavior of the PA6−30PF and PA6−30PF-5CNC composites. (a) Frequency sweep test at a fixed strain amplitude of 1% at 240 °C. (b) Flow curve test at 240 °C. Based on the plots, it can be observed that the storage modulus of the polymer composite increases with the addition of CNC. The increase in viscosity was not significant, which indicates that the processability of the composite is maintained.

https://doi.org/10.1021/acssuschemeng.3c06351
ACS Sustainable Chem. Eng. 2024, 12, 490−500

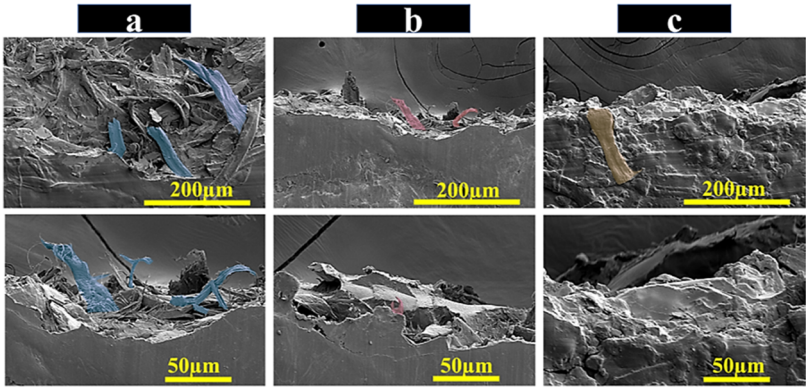

Figure 8. SEM micrographs of the fractured surfaces of (a) PA6−30PF(HM), (b) PA6−30PF, and (c) PA6−30PF-5CNC after 30 min of premixing ball milling. Different colors are employed to distinguish various fiber morphologies on the fracture surface.

size of the agglomerates and increasing the number of individual PFs dispersed. Consequently, the interparticle distances reduced in hybrid structure, resulting in a stronger material. This is more likely to lead to a decrease in the number of pulled-out fibers and an increase in the stacking of PFs within the polymers.

3.9. Water Uptake Capacity. The assessment of water absorption in composites reinforced with natural fibers is crucial as it is often linked to problems with dimensional stability and a reduction in mechanical properties.[42,48] As shown in Figure 9, this highlights the significance of evaluating

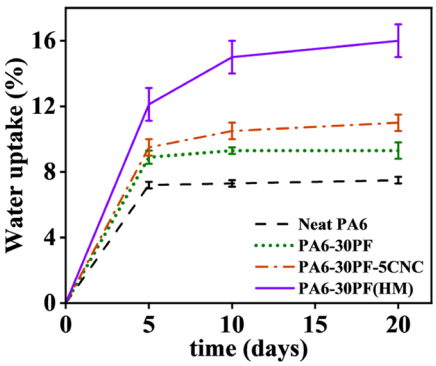

Figure 9. Water uptake behavior of neat PA6, PA6−30PF, PA6−30PF-5CNC, and PA6−30PF(HM). As shown in the plot, the hand-mixed sample exhibited higher water uptake at the same concentration of pulp fiber compared with the sample prepared using ball milling.

the water absorption in such materials. After being immersed for 20 days in water, the neat PA6 matrices used in this study exhibited a water absorption of under 8 ± 0.1% confirming their somewhat hydrophilic nature due to the existence of carboxyl groups at the end of their chains. The higher water absorptions observed in the composites in this study regardless of the preparation method can be attributed to the high affinity of cellulose for water. This is a well-established phenomenon, as it is generally agreed upon that the addition of hydrophilic components to composites results in increased water absorption. Furthermore, the water uptake behavior of all composites in this study exhibited a similar pattern, with a rapid increase in the first few days of immersion, followed by stabilization after reaching saturation.[22]

We compared PA6 reinforced with 30 wt% PF that was prepared with and without premixing using planetary ball milling. The results indicate that the premixed composite sample exhibited lower water absorption levels (50%) than those of the PA6−30PF (HM) sample. The positive impact of premixing on the water uptake behavior observed in this study aligns with the thermomechanical property results, suggesting that premixing ball milling facilitates the embedment and improved dispersion of PFs in the matrix, promoting their effective integration and reducing the ease of water permeation into the composite.

The introduction of 5 wt % CNC to the PA6-PFs composite prepared via premixing ball milling resulted in a lower water uptake compared to that of the PA6−30PF (HM) sample despite the CNC's hydrophilic nature and the fact that its addition increases the interaction between the composite and moisture by providing more hydrogen bonding sites. Overall, the premixed sample demonstrated a lower sensitivity to moisture compared with the PA6−30PF (HM) sample, as evidenced by its lower water uptake. In our previous work,[6] we suggested that the lower water uptake of the premixed sample can be attributed to its higher degree of crystallinity compared to the HM sample. Polymer composites with high crystallinity typically exhibit lower permeability due to tightly packed polymer chains, which can prevent water penetration. Additionally, Aiken, Doty, and Mark[49] found that moisture tends to be absorbed by the amorphous areas in polymer composites.

4. CONCLUSIONS

The present work elaborates on how sequential ball milling could be employed to facilitate the fabrication of highly advanced bioreinforced composites for the proposed applications in the automotive industry. The designed composites enjoyed facilitated processing, high mechanical properties, and biodegradability, coming from the unique features of sequential ball milling. Accordingly, the polymer composite, derived from premixing the ball milling of PA6 and PFs, exhibits heightened thermal stability. This feature increased the applicability of postprocessing at high temperatures, e.g., compression molding, known as one of the most widely used manufacturing processes for composite shaping. Through the strategic incorporation of a cellulose nanocrystal (CNC) modifying agent, we successfully address void spaces between the fiber and matrix, leading to increased packing density. The incorporation of micronized fibers significantly enhances the Young's modulus. Notably, a sample with 30 wt % PFs displays

https://doi.org/10.1021/acssuschemeng.3c06351
ACS Sustainable Chem. Eng. 2024, 12, 490−500

a notable modulus of 3.9 GPa, marking a 160% enhancement compared to the neat PA6 sample (1.5 GPa). Upon adding 5 wt % CNC modifying agent to the samples holding 30 wt % PFs, Young's modulus further improved to 4.3 GPa. Rheology results indicate that adding CNCs using milling does not adversely affect the melt processability of the composites. Through the application of ball milling, we have succeeded in elevating the concentration of biobased fillers without any compromise on mechanical properties. This development is highly significant, as it paves the way for substituting petroleum-based components with more sustainable alternatives. Our approach showcases the potential for heightened sustainability without any sacrifice in performance. Additionally, our premixing ball milling technique conferred enhanced moisture resistance to the inherently hydrophilic PA6-PFs composite. For instance, the sample made through sequential milling of PA6−30PF displayed 50% lower water absorption compared with a sample that was hand-mixed but used the same components. Collectively, these findings demonstrate that sequential ball milling coupled with the use of CNC modifying agents can significantly improve the mechanical, thermal, and rheological properties of natural fiber-reinforced composites. This contributes to broadening their applicability, making them more competitive alternatives to traditional composites and polymers.

■ ASSOCIATED CONTENT

Supporting Information

The Supporting Information is available free of charge at https://pubs.acs.org/doi/10.1021/acssuschemeng.3c06351.

Optimization of premixing ball milling, effect of milling time on thermomechanical properties, TGA, DMTA, tensile test, results of the analysis of variance (ANOVA), morphological analysis of pulp fibers, and mathematical modeling of milling time (PDF)

■ AUTHOR INFORMATION

Corresponding Author

E. Johan Foster − *Department of Chemical and Biological Engineering, BioProducts Institute, University of British Columbia, Vancouver, British Columbia V6T 1Z3, Canada;* orcid.org/0000-0002-4103-8510; Email: johan.foster@ubc.ca

Author

Adel Jalaee − *Department of Chemical and Biological Engineering, BioProducts Institute, University of British Columbia, Vancouver, British Columbia V6T 1Z3, Canada*

Complete contact information is available at: https://pubs.acs.org/10.1021/acssuschemeng.3c06351

Notes

The authors declare no competing financial interest.

■ ACKNOWLEDGMENTS

The authors gratefully acknowledge the financial support provided by the NSERC Canfor Industrial Research Chair in Advanced Bioproducts, (# 553449−19), NSERC Discovery Grant (RGPIN-2021−03172), the Canada Foundation for Innovation (Project number 022176), and the Pacific Economic Development Canada (PacifiCan). They also thank AdvanSix for the provision of PA6 pellets and Prof. Orlando Rojas, Prof. Scott Rennackar, Prof. Savvas Hatzikiriakos, and Prof. Milad Kamkar for their conversation and support via instrument access. Finally, the authors extend their appreciation to Farhad Ahmadijokani, Victoria French, and Ran Bi for their kind assistance.

■ REFERENCES

(1) Ferreira, F. V.; Pinheiro, I. F.; de Souza, S. F.; Mei, L. H.; Lona, L. M. Polymer composites reinforced with natural fibers and nanocellulose in the automotive industry: A short review. *J. Compos. Sci.* **2019**, *3* (2), No. 51.

(2) Thakur, V. K.; Thakur, M. K.; Raghavan, P.; Kessler, M. R. Progress in Green Polymer Composites from Lignin for Multifunctional Applications: A Review. *ACS Sustainable Chem. Eng.* **2014**, *2* (5), 1072−1092.

(3) Global Biocomposites Market Size, 2023 https://www.globenewswire.com. (accessed August 17, 2023).

(4) Elsabbagh, A.; Steuernagel, L.; Ring, J. Natural Fibre/PA6 composites with flame retardance properties: Extrusion and characterisation. *Composites, Part B* **2017**, *108*, 325−333.

(5) De Carvalho, A. J. F.; Curvelo, A. A. S.; Agnelli, J. A. M. Wood pulp reinforced thermoplastic starch composites. *Int. J. Polym. Mater.* **2002**, *51* (7), 647−660.

(6) Jalaee, A.; Kamkar, M.; French, V.; Rojas, O. J.; Foster, E. J. Direct milling: Efficient, facile, and green method for processing fibrillated cellulose/polymeric nanocomposites with boosted thermomechanical and rheological performance. *Carbohydr. Polym.* **2023**, *314*, No. 120932.

(7) Bio-composites for cars, 2018 https://www.allthings.bio/bio-composites-for-cars.

(8) Fazeli, M.; Florez, J. P.; Simão, R. A. Improvement in adhesion of cellulose fibers to the thermoplastic starch matrix by plasma treatment modification. *Composites, Part B* **2019**, *163*, 207−216.

(9) Shi, S.; Yang, C.; Nie, M. Enhanced interfacial strength of natural fiber/polypropylene composite with mechanical-interlocking interface. *ACS Sustainable Chem. Eng.* **2017**, *5* (11), 10413−10420.

(10) Nicharat, A.; Sapkota, J.; Weder, C.; Foster, E. J. Melt processing of polyamide 12 and cellulose nanocrystals nanocomposites. *J. Appl. Polym. Sci.* **2015**, *132* (45), No. 42752.

(11) Venkatraman, P.; Trotto, E.; Burgoyne, I.; Foster, E. J. Premixed cellulose nanocrystal reinforcement of polyamide 6 for melt processing. *Polym. Compos.* **2020**, *41* (10), 4353−4361.

(12) (a) Dhumpa, R.; Foster, J. *High-Performance Nanocellulose Composite for Aviation and Aerospace*; Innovatech Engineering LLC: Tallahassee, FL (United States), 2018. (b) Zhu, R.; Yadama, V.; Liu, H.; Lin, R. J.; Harper, D. P. Fabrication and characterization of Nylon 6/cellulose nanofibrils melt-spun nanocomposite filaments. *Composites, Part A* **2017**, *97*, 111−119.

(13) Sessini, V.; Haseeb, B.; Boldizar, A.; Re, G. L. Sustainable pathway towards large scale melt processing of the new generation of renewable cellulose−polyamide composites. *RSC Adv.* **2021**, *11* (2), 637−656.

(14) Herrera, N.; Olsén, P.; Berglund, L. A. Strongly Improved Mechanical Properties of Thermoplastic Biocomposites by PCL Grafting inside Holocellulose Wood Fibers. *ACS Sustainable Chem. Eng.* **2020**, *8* (32), 11977−11985.

(15) Xanthopoulou, E.; Chrysafi, I.; Polychronidis, P.; Zamboulis, A.; Bikiaris, D. N. Evaluation of eco-friendly hemp-fiber-reinforced recycled HDPE composites. *J. Compos. Sci.* **2023**, *7* (4), No. 138.

(16) Chakrabarty, A.; Teramoto, Y. Recent advances in nanocellulose composites with polymers: a guide for choosing partners and how to incorporate them. *Polymers* **2018**, *10* (5), No. 517.

(17) Xu, S.; Fang, Y.; Yi, S.; He, J.; Zhai, X.; Song, Y.; Wang, H.; Wang, Q. Effects of lithium chloride and chain extender on the properties of wood fiber reinforced polyamide 6 composites. *Polym. Test.* **2018**, *72*, 132−139.

(18) Taheri, H.; Hietala, M.; Suopajärvi, T.; Liimatainen, H.; Oksman, K. One-Step Twin-Screw Extrusion Process to Fibrillate

Deep Eutectic Solvent-Treated Wood to Be Used in Wood Fiber-Polypropylene Composites. *ACS Sustainable Chem. Eng.* **2021**, *9* (2), 883−893.
(19) Sridhara, P. K.; Vilaseca, F. High performance PA 6/cellulose nanocomposites in the interest of industrial scale melt processing. *Polymers* **2021**, *13* (9), No. 1495.
(20) Venkatraman, P.; Gohn, A. M.; Rhoades, A. M.; Foster, E. J. Developing high performance PA 11/cellulose nanocomposites for industrial-scale melt processing. *Composites, Part B* **2019**, *174*, No. 106988.
(21) Zhang, F. L.; Zhu, M.; Wang, C. Y. Parameters optimization in the planetary ball milling of nanostructured tungsten carbide/cobalt powder. *Int. J. Refract. Met. Hard Mater.* **2008**, *26* (4), 329−333.
(22) Valente, B. F. A.; Silvestre, A. J.; Neto, C. P.; Vilela, C.; Freire, C. S. R. Effect of the micronization of pulp fibers on the properties of green composites. *Molecules* **2021**, *26* (18), No. 5594.
(23) (a) Agrawala, S.; Rajamani, R. K.; Songfack, P.; Mishra, B. K. Mechanics of media motion in tumbling mills with 3d discrete element method. *Miner. Eng.* **1997**, *10* (2), 215−227. (b) Maleki-Moghaddam, M.; Yahyaei, M.; Banisi, S. A method to predict shape and trajectory of charge in industrial mills. *Miner. Eng.* **2013**, *46*−*47*, 157−166.
(24) Bailey, E. J.; Winey, K. I. Dynamics of polymer segments, polymer chains, and nanoparticles in polymer nanocomposite melts: A review. *Prog. Polym. Sci.* **2020**, *105*, No. 101242.
(25) Yousefian, H.; Rodrigue, D. Effect of nanocrystalline cellulose on morphological, thermal, and mechanical properties of nylon 6 composites. *Polym. Compos.* **2016**, *37* (5), 1473−1479.
(26) Nicharat, A.; Sapkota, J.; Foster, E. J. Pre-mixing and masterbatch approaches for reinforcing poly(vinyl acetate) with cellulose based fillers. *Ind. Crops Prod.* **2016**, *93*, 244−250.
(27) Zhu, Y.-g.; Li, Z.-Q.; Zhang, D.; Tanimoto, T. Structural changes in poly (ethylene terephthalate) induced by cryomilling and ambimilling. *J. Polym. Sci., Part B: Polym. Phys.* **2006**, *44* (6), 986−993.
(28) Maleki-Moghaddam, M.; Yahyaei, M.; Banisi, S. A method to predict shape and trajectory of charge in industrial mills. *Miner. Eng.* **2013**, *46*−*47*, 157−166.
(29) Sridhara, P. K.; Masso, F.; Olsén, P.; Vilaseca, F. Strong polyamide-6 nanocomposites with cellulose nanofibers mediated by green solvent mixtures. *Nanomaterials* **2021**, *11* (8), No. 2127.
(30) Espinach, F.; Boufi, S.; Delgado-Aguilar, M.; Julián, F.; Mutjé, P.; Méndez, J. Composites from poly (lactic acid) and bleached chemical fibres: Thermal properties. *Composites, Part B* **2018**, *134*, 169−176.
(31) Pritchard, C. Q.; Funk, G.; Owens, J.; Stutz, S.; Gooneie, A.; Sapkota, J.; Foster, E. J.; Bortner, M. J. Adjustable film properties of cellulose nanofiber and cellulose nanocrystal composites. *Carbohydr. Polym.* **2022**, *286*, No. 119283.
(32) Aitha, S.; Vasanthan, N. Effect of cellulose nanocrystals on crystallization, morphology and phase transition of polyamide 6. *Compos. Interfaces* **2020**, *27* (4), 371−384.
(33) Kiziltas, A.; Nazari, B.; Gardner, D. J.; Bousfield, D. W. Polyamide 6−cellulose composites: effect of cellulose composition on melt rheology and crystallization behavior. *Polym. Eng. Sci.* **2014**, *54* (4), 739−746.
(34) Ahmadijokani, F.; Shojaei, A.; Arjmand, M.; Alaei, Y.; Yan, N. Effect of short carbon fiber on thermal, mechanical and tribological behavior of phenolic-based brake friction materials. *Composites, Part B* **2019**, *168*, 98−105.
(35) Ahmadijokani, F.; Alaei, Y.; Shojaei, A.; Arjmand, M.; Yan, N. Frictional behavior of resin-based brake composites: Effect of carbon fibre reinforcement. *Wear* **2019**, *420*−*421*, 108−115.
(36) Sonseca, Á.; Sahuquillo, O.; Foster, E. J.; Giménez, E. Mechanical properties and degradation studies of poly (mannitol sebacate)/cellulose nanocrystals nanocomposites. *RSC Adv.* **2015**, *5* (69), 55879−55891.
(37) Gojny, F. H.; Wichmann, M. H. G.; Fiedler, B.; Bauhofer, W.; Schulte, K. Influence of nano-modification on the mechanical and electrical properties of conventional fibre-reinforced composites. *Composites, Part A* **2005**, *36* (11), 1525−1535.
(38) Lee, J.-A.; Yoon, M.-J.; Lee, E.-S.; Lim, D.-Y.; Kim, K.-Y. Preparation and characterization of cellulose nanofibers (CNFs) from microcrystalline cellulose (MCC) and CNF/polyamide 6 composites. *Macromol. Res.* **2014**, *22*, 738−745.
(39) (a) Qiang, T.; Wang, J.; Wolcott, M. P. Facile fabrication of 100% bio-based and degradable ternary cellulose/PHBV/PLA composites. *Materials* **2018**, *11* (2), No. 330. (b) Qiang, T.; Wang, J.; Wolcott, M. P. Facile preparation of cellulose/polylactide composite materials with tunable mechanical properties. *Polym.-Plast. Technol. Eng.* **2018**, *57* (13), 1288−1295.
(40) Liu, L.; Grunlan, J. C. Clay assisted dispersion of carbon nanotubes in conductive epoxy nanocomposites. *Adv. Funct. Mater.* **2007**, *17* (14), 2343−2348.
(41) Dang, Z.-M.; Yao, S.-H.; Yuan, J.-K.; Bai, J. Tailored dielectric properties based on microstructure change in BaTiO3-carbon nanotube/polyvinylidene fluoride three-phase nanocomposites. *J. Phys. Chem. C* **2010**, *114* (31), 13204−13209.
(42) Vlasveld, D. P. N.; Groenewold, J.; Bersee, H. E. N.; Picken, S. J. Moisture absorption in polyamide-6 silicate nanocomposites and its influence on the mechanical properties. *Polymer* **2005**, *46* (26), 12567−12576.
(43) Sapkota, J.; Natterodt, J. C.; Shirole, A.; Foster, E. J.; Weder, C. Fabrication and properties of polyethylene/cellulose nanocrystal composites. *Macromol. Mater. Eng.* **2017**, *302* (1), No. 1600300.
(44) Kamkar, M.; Aliabadian, E.; Zeraati, A. S.; Sundararaj, U. Application of nonlinear rheology to assess the effect of secondary nanofiller on network structure of hybrid polymer nanocomposites. *Phys. Fluids* **2018**, *30* (2), No. 023102.
(45) Sultana, S. M. N.; Pawar, S. P.; Kamkar, M.; Sundararaj, U. Tailoring MWCNT dispersion, blend morphology and EMI shielding properties by sequential mixing strategy in immiscible PS/PVDF blends. *J. Electron. Mater.* **2020**, *49*, 1588−1600.
(46) Kamkar, M.; Salehiyan, R.; Goudoulas, T. B.; Abbasi, M.; Saengow, C.; Erfanian, E.; Sadeghi, S.; Natale, G.; Rogers, S. A.; Giacomin, A. J.; Sundararaj, U. Large amplitude oscillatory shear flow: Microstructural assessment of polymeric systems. *Prog. Polym. Sci.* **2022**, *132*, No. 101580.
(47) Kuram, E.; Sarac, L.; Ozcelik, B.; Yilmaz, F. Mechanical, chemical, thermal, and rheological properties of recycled PA6/ABS binary and PA6/PA66/ABS ternary blends. *J. Appl. Polym. Sci.* **2014**, *131* (18), No. 40810.
(48) Peng, Y.; Nair, S. S.; Chen, H.; Yan, N.; Cao, J. Effects of Lignin Content on Mechanical and Thermal Properties of Polypropylene Composites Reinforced with Micro Particles of Spray Dried Cellulose Nanofibrils. *ACS Sustainable Chem. Eng.* **2018**, *6* (8), 11078−11086.
(49) Morgan, P. W. Structure and moisture permeability of film-forming polymers. *Ind. Eng. Chem.* **1953**, *45* (10), 2296−2306.

https://doi.org/10.1021/acssuschemeng.3c06351
ACS Sustainable Chem. Eng. 2024, 12, 490−500